Journal of
Materials Chemistry A

PAPER

View Article Online
View Journal | View Issue

Cite this: *J. Mater. Chem. A*, 2014, **2**, 20776

High voltage in hole conductor free organo metal halide perovskite solar cells†

Alex Dymshits, Amit Rotem and Lioz Etgar*

Received 20th October 2014
Accepted 21st October 2014

DOI: 10.1039/c4ta05613b

www.rsc.org/MaterialsA

Organo metal halide perovskite has attracted considerable attention recently due to its distinctive properties that make it especially useful in photovoltaic solar cells. In this work we demonstrate high open circuit voltage of 1.35 V using $Al_2O_3/CH_3NH_3PbBr_3$ perovskite solar cells without a hole conductor. The contact potential difference under light measured by surface photovoltage spectroscopy of $CH_3NH_3PbBr_3$ was more than twice that of $CH_3NH_3PbI_3$, which results in smaller surface potential for the $Al_2O_3/CH_3NH_3PbBr_3$ cells. Incident modulated photovoltage spectroscopy shows a longer recombination lifetime for the $Al_2O_3/CH_3NH_3PbBr_3$ cells than for the $TiO_2/CH_3NH_3PbI_3$ cells or for the $TiO_2/CH_3NH_3PbBr_3$ cells, further supporting the high open circuit voltage. The possibility to gain high open circuit voltage even without a hole transport material in perovskite solar cells shows that the perovskite/metal oxide interface has a major effect on the open circuit voltage in perovskite based solar cells.

Introduction

Alternative energy is an important research area and will remain so for the foreseeable future, and photovoltaics (PV) is a key technology for a sustainable energy supply. A PV device is based on the photoelectric effect, requiring photo-generation of charge carriers (electrons and holes) in a light-absorbing material and their separation to conductive contacts that transmit electricity. A breakthrough has occurred in recent years as a promising new material, organo metal halide perovskite, is being used in the solar cells, achieving approximately 18% efficiency.[1] Interestingly, the perovskite isn't restricted to a specific solar cell architecture and can be used with different metal oxides; where injection of electrons is possible and where the metal oxide functions as a scaffold.[2–4] Moreover, a long-range electron–hole diffusion length was found in an organo metal perovskite absorber, which might explain the high efficiency achieved for perovskite based solar cells.[5,6] Other reports demonstrate that the use of the perovskite both as a light harvester and as a hole conductor; eliminating the use of hole transport material (HTM) and achieving more than 10% efficiency.[7–9]

One of the attractive properties of organo metal halide perovskite is its ability to gain high open circuit voltage (V_{oc}) with a high ratio of qV_{oc}/E_g. V_{oc} of 1.15 V was achieved with a cell that used $CH_3NH_3PbBr_3$ as sensitizer/absorber, with poly[*N*-9-hepta-decanyl-2,7-carbazole-*alt*-3,6-bis-(thiophen-5-yl)-2,5-dioctyl-2,5-dihydropyrrolo[3,4-]pyrrole-1,4-dione] (PCBTDPP) as the hole transport material.[10] An even higher open circuit voltage of 1.3 V was the result when using *N*,*N*′-dialkylperylenediimide (PDI) as the hole transport material with $CH_3NH_3PbBr_3$ as the sensitizer/absorber.[11] Recently 1.5 V was reported when using $CH_3NH_3PbBr_{3-x}Cl_x$ with 4,4′-bis(*N*-carbazolyl)-1,1′-biphenyl (CBP) as the hole conductor.[12] Both high efficiency (6.7%) and high voltage (1.4 V) was demonstrated with hole transport material based on tri-arylamine (TAA) polymer derivatives containing fluorene and indenofluorene.[13] All the reports mentioned, relating to high voltage based on perovskite use hole transport material to tune and to gain high V_{oc}. However, is it possible to get high V_{oc} without hole transport material? Based on recent reports,[12,13] the voltage in the perovskite solar cells isn't determined simply by the difference between the TiO_2 Fermi level and the Fermi level of the HTM. Therefore, it could be that high V_{oc} can be achieved in perovskite based solar cells even without HTM.

In this work, we demonstrate a high V_{oc} of 1.35 V for perovskite solar cells without a hole conductor. Several combinations of metal oxides/perovskites are studied. Surface photovoltage and incident modulated photovoltage spectroscopy are used to elucidate the reason for the high voltage achieved for these hole conductor free cells.

Results and discussion

Fig. 1a shows a schematic illustration of the high voltage hole conductor free perovskite solar cell. The bottom layer is composed of conductive glass with a TiO_2 compact layer; then a

---

The Hebrew University of Jerusalem, Institute of Chemistry, Casali Center for Applied Chemistry, Jerusalem 91904, Israel. E-mail: lioz.etgar@mail.huji.ac.il

† Electronic supplementary information (ESI) available. See DOI: 10.1039/c4ta05613b

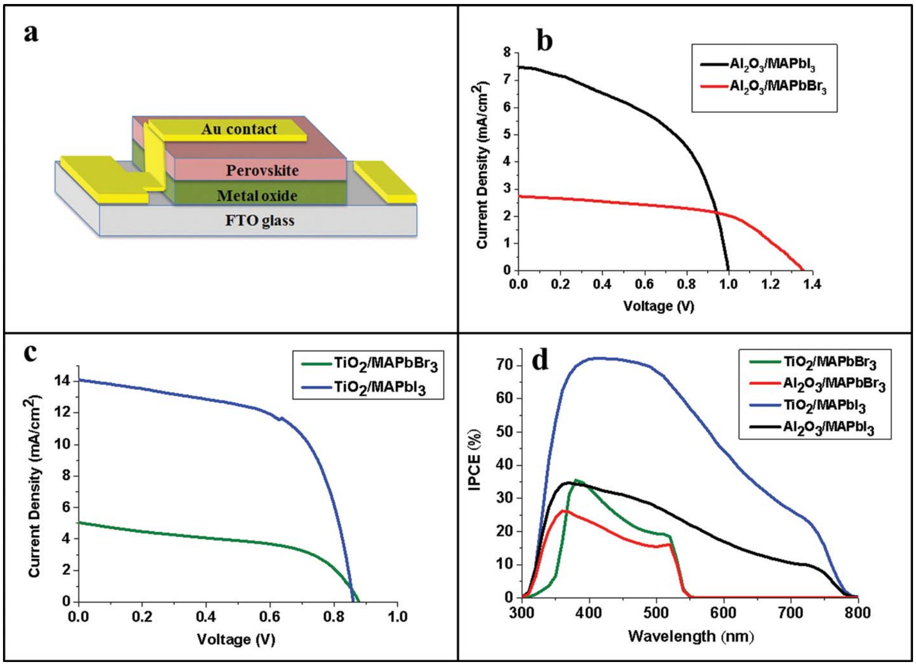

Fig. 1 (a) The solar cell structure. (B) *JV* curves of the cells made with Al_2O_3 as a scaffold. (c) Cells made with TiO_2. (d) The corresponding IPCE curves.

thin film of nanocrystalline metal oxide TiO_2 or Al_2O_3 was deposited on top. The $CH_3NH_3PbI_3$ or $CH_3NH_3PbBr_3$ (CH_3NH_3 = MA) perovskites were deposited by the two-step deposition as described earlier.[14,15] Finally, a metal contact was evaporated directly on top of the perovskite. As our previous work shows,[9] the perovskite functions both as light harvester and hole conductor, eliminating the use of a hole transport material.

Fig. 1b–d and Table 1 present the photovoltaic parameters and the incident photon to current efficiency (IPCE) achieved for the high voltage cells. Four different combinations were studied—nanocrystalline TiO_2 with $MAPbI_3$ and $MAPbBr_3$, and nanocrystalline Al_2O_3 with both perovskites. The open circuit voltage (V_{oc}) for the cells with the $MAPbBr_3$ perovskite delivers higher voltages compared to the cells with the $MAPbI_3$ perovskite related to the same metal oxide. Moreover, the cells with Al_2O_3 achieve higher V_{oc} compared to the TiO_2 based cells. The highest V_{oc} observed for the $Al_2O_3/MAPbBr_3$ configuration achieved 1.35 V without a hole conductor. This is the highest reported open circuit voltage for perovskite cells without a hole conductor and is comparable to cells using hole transport material. It is important to note that the average V_{oc} (including more than 11 cells) for the $Al_2O_3/MAPbBr_3$ configuration is 1.24 ± 0.08 V with 4 cells having V_{oc} of more than 1.3 V and 4 cells with V_{oc} higher than 1.21 V.

Table 1 Photovoltaic parameters of the hole conductor free solar cells studied

	η (%)	Fill factor	J_{sc} (mA cm^{-2})	V_{oc} (V)
$TiO_2/MAPbI_3$	7.5	0.61	14.1	0.86
$TiO_2/MAPbBr_3$	1.88	0.49	4.37	0.87
$Al_2O_3/MAPbI_3$	4.13	0.5	7.46	1.0
$Al_2O_3/MAPbBr_3$	2.02	0.55	2.7	1.35

High power conversion efficiency (PCE) with high voltage was observed for the $Al_2O_3/MAPbI_3$ configuration achieving PCE of 4.1% with V_{oc} of 1 V. The IPCE spectra show typical behavior with coverage until 550 nm wavelength for the $MAPbBr_3$ and until 780 nm wavelength for the $MAPbI_3$.

Fig. 2a–b show the energy level diagram for the four different cases described in this paper. Fig. 2a presents the $MAPbBr_3$ and $MAPbI_3$ deposited on Al_2O_3, which function as a scaffold; electron injection from the perovskite to the Al_2O_3 isn't possible in this configuration. Fig. 2b presents the $MAPbBr_3$ and $MAPbI_3$ with TiO_2, where electron injection from the perovskite to the TiO_2 is favorable. Surface photovoltage (SPV) was used to measure the work function of the Al_2O_3, TiO_2, $MAPbI_3$ and $MAPbBr_3$; the calculated work functions are shown as red lines in Fig. 2. The work function positions (which are the Fermi level positions) correspond well to the p-type behavior of the $MAPbBr_3$ and $MAPbI_3$ perovskites, and the n-type behavior of the TiO_2 as discussed below. Fig. 2c and d show the corresponding high resolution scanning electron microscopy (HR-SEM) cross sections of the $Al_2O_3/MAPbI_3$ and $Al_2O_3/MAPbBr_3$ HTM free cells, the perovskite over layer can be observed clearly. The HR-SEM cross sections of the TiO_2 based cells are shown in the ESI. (Fig. 2S†)

Surface photovoltage (SPV) spectroscopy and incident modulated photovoltage spectroscopy (IMVS) were performed to gain more information about the reason for the high open circuit voltage when no HTM is used. Previous studies already demonstrate high V_{oc} in perovskite cells contain HTM. It was

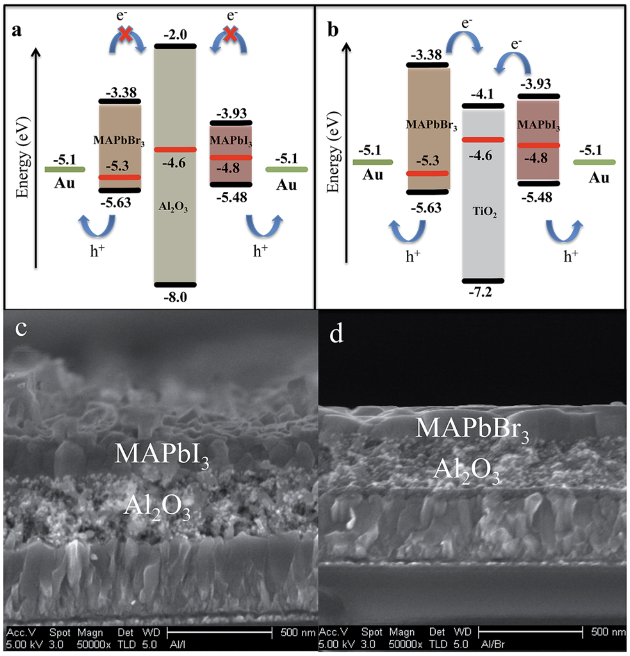

Fig. 2 (a and b) Energy level diagram of the different cells. Fermi levels measured under dark are presented in red in the figure. The position of the conduction and valence bands are according to ref. 13. (c) HR-SEM cross section of the $Al_2O_3/MAPbI_3$ HTM free cell. (d) HR-SEM cross section of the $Al_2O_3/MAPbBr_3$ HTM free cell.

suggested that the V_{oc} is not merely the difference between the hole Fermi level of the hole conductor and the electron Fermi level of the nanocrystalline TiO_2.[13,16] Moreover, it was reported that charges could be accumulated in the perovskite due to its high capacitance, which allows the control of the quasi Fermi level during illumination.[17]

The SPV technique is based on a Kelvin probe, which measures the difference in work functions (also known as the contact potential difference (CPD)) between a metallic reference probe and semiconductor surface. The metallic probe vibrates, which forms a capacitor arrangement between the reference electrode and the semiconductor (the distance between them is a few millimeter). This results in an AC current in the external circuit. If there is no charge on the capacitor, the AC current is zero. In this case, the CPD must be zero. The AC current nullifies when a DC bias is applied. Thus, the applied DC bias is equal and opposite to the CPD (please see Fig. 3S in the ESI† for schematic explanation).

The SPV spectra of the $MAPbI_3$ and $MAPbBr_3$ are shown in Fig. 3a, with the estimated band gaps shown as vertical lines. Several observations result from the SPV spectra (Fig. 3a). First, the spectra provide information about the band gaps of the materials, equivalent to the information observed from the absorption spectra (Fig. S1 in the ESI†). Second, the sign of the SPV signal indicates the samples type. The surface work function is changed on illumination. It decreases for the n-type semiconductor—TiO_2 in this case—and increases for the p-type semiconductor, the $MAPbI_3$ and $MAPbBr_3$ in this case. A third important observation is related to the unique property of the SPV method, its immunity to reflection or scattering losses, only photons that are absorbed in the sample contribute to the SPV signal. In this case the signal onset starts at photon energies very close to the band gap of the perovskite samples (the $MAPbI_3$ and the $MAPbBr_3$), and as a result, it can be concluded that the perovskite samples have fewer sub-bandgap states. The relation qV_{oc}/E_g is the ratio of the maximum voltage developed by the solar cell (V_{oc}) to the voltage related to the band-gap of the absorber (E_g/q). For the $Al_2O_3/MAPbBr_3$ cell the qV_{oc}/E_g is 0.61, compared to recent reports of high voltage perovskite cells with HTM shown as qV_{oc}/E_g of 0.55 and 0.73.[11,12] Our results demonstrate comparable values with respect to the values obtained with HTM.

The qV_{oc}/E_g relation in the case of the Al_2O_3 based cells are 0.64 and 0.61 for the $MAPbI_3$ and $MAPbBr_3$, respectively, and for the TiO_2 based cells, 0.55 and 0.37 for $MAPbI_3$ and $MAPbBr_3$, respectively. Based on these values it can be observed that the $Al_2O_3/MAPbBr_3$ based cells have slightly more thermal losses than the $Al_2O_3/MAPbI_3$ cells, moreover high thermal losses were observed in the TiO_2 based cell compared to the Al_2O_3 based cells.

Fig. 3b presents the contact potential difference (CPD) change when a light is switched on and off. The SPV onset t_{on} and t_{off} are below the resolution limit of the measurement system. Our observations from these measurements are related to the change in the CPD—for the TiO_2 sample, a negative change in the CPD was observed, while for the perovskites samples, a positive change in the CPD was observed, corresponding to their electronic behavior. The ΔCPD for the $MAPbI_3$ is 350 mV and the ΔCPD for the $MAPbBr_3$ is 850 mV.

The V_S presented in Fig. 3c and d is the surface potential barrier (where V_{sd} is the surface potential in the dark and V_{sl} is the surface potential in the light), which was measured in the SPV experiment. The difference between the surface potential in the light (V_{sl}) and in the dark (V_{sd}) is defined as the SPV signal. In a super band gap, illumination photons with energy equal or larger than the band gap, hit the material and generate electron–hole pairs which is collected by the surface barrier, consequently the surface potential is reduced. The trap to band transition is neglected in super band gap illumination while the band-to-band absorption is the dominant one.

Fig. 3c and d shows the effect of band-to-band transition on the SPV response of $MAPbBr_3$ and $MAPbI_3$, respectively. Under illumination, there is redistribution of surface charges, which decrease the band bending, and as a result the SPV response is generated. According to the ΔCPD shown in Fig. 3b the surface potential for the $MAPbBr_3$ is smaller than the surface potential for the $MAPbI_3$ as indicated by the bi directional arrow in Fig. 3c and d, respectively (this is also seen by the bend bending reduction, since the difference between V_{sl} to V_{sd} is larger in the case of $MAPbBr_3$). The reduction of the surface potential observed from the SPV measurements for the HTM free $MAPbBr_3$ cells, could be a possible contribution to the higher V_{oc} achieved for these cells.

Further contribution to the difference in the open circuit voltage is presented in Fig. 4. The recombination lifetime (τ_r) as a function of the voltage were calculated by IMVS.[18–20] All cells

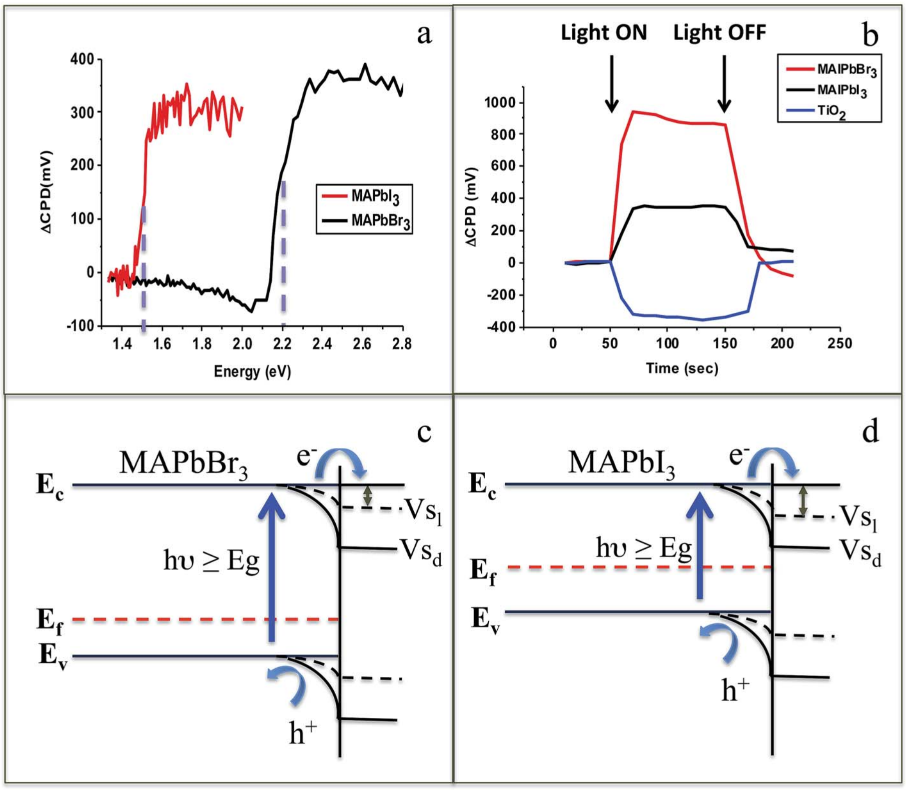

Fig. 3 (a) SPV spectra of the $MAPbI_3$ and $MAPbBr_3$ films with estimated band gaps, 1.55 eV and 2.2 eV, respectively. (b) Contact potential difference (CPD) change with white light switched on and off for the samples studied. (c) The effect of band-to-band transitions on the surface photovoltage responses of $MAPbBr_3$ and (d) $MAPbI_3$. V_{sd}-surface potential in the dark, V_{sl}-surface potential in the light.

showed the same dependence of electron recombination lifetime (which are the minority carriers) by the voltage; the decrease of the recombination lifetime with increasing the voltage. This behavior can be attributed to the increased recombination with the higher electron density.[18] However, the τ_r values are different for the various cells; in particular, the lower τ_r values were observed for the $TiO_2/MAPbI_3$ cell, which also had the lower V_{oc}. The highest τ_r values were observed for the $Al_2O_3/MAPbBr_3$ cell which resulted in less recombination (since the lifetime for recombination is longer) corresponding with the highest voltage observed. Longer recombination lifetime (τ_r) will decrease the recombination which can result in higher V_{oc}.[21,22] In addition, longer recombination lifetimes were observed for the cells with the Al_2O_3 as the scaffold, compared to cells with mesoporous TiO_2, which could contribute to the higher voltages observed in the case of Al_2O_3 based cells. This is consistent with the qV_{oc}/E_g relation as discussed above, where more thermal losses were observed for cells based on TiO_2 as the metal oxide compare to Al_2O_3 based cells.

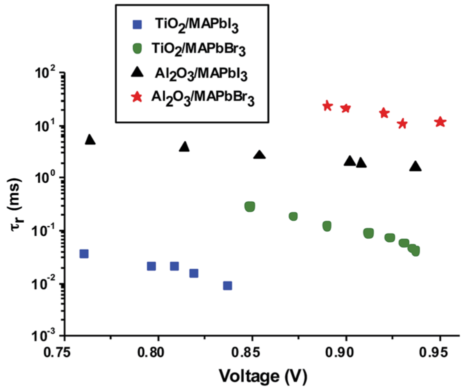

Fig. 4 Recombination lifetime (τ_r) as a function of the open circuit voltage for the cells studied, measured by IMVS.

Conclusions

In this work, high voltage of 1.35 V was observed for hole conductor free perovskite solar cells. SPV and IMVS techniques were used to elucidate the origin of the high voltage observed. The Fermi level position and the SPV spectra of the $MAPbI_3$ and $MAPbBr_3$ reveal the p-type behavior of these perovskites. The CPD change when light was switched on and off was higher by a factor of 2.5 for the $MAPbBr_3$ cells compared to the $MAPbI_3$ cells. The change in the CPD during illumination resulted in smaller surface potential for the $Al_2O_3/MAPbBr_3$ cells which could contribute to the higher open circuit voltage achieved in the $MAPbBr_3$ cells. Further support was observed by longer recombination lifetime for the Al_2O_3 based cells, compared to cells with mesoporous TiO_2. The high open circuit voltage observed in cells without a hole conductor indicates that the origin of the open circuit voltage is affected by the perovskite and the perovskite/metal oxide interface.

Experimental

Material synthesis

The Al_2O_3 nanoparticles (<50 nm particle size, Sigma-Aldrich) were dissolved in isopropanol at a concentration of 20 wt%. The Al_2O_3 nanoparticles were deposited by spin coating at 2000 r.p.m. for 10 s and annealed at 500 °C for 30 min. For the TiO_2 films DYESOL DSL 90-T paste was used. The TiO_2 paste was diluted in ethanol in a ratio of 1 : 4 by weight. The deposition and the annealing conditions were the same as for the Al_2O_3.

CH_3NH_3I and CH_3NH_3Br were synthesized as described previously[23,24] by reacting 30 mL of methylamine (40% in methanol, TCI) and 32.3 mL of hydroiodic acid (57 wt% in water, Aldrich) or 23.32 mL of hydrobromic acid (48 wt% in water, Aldrich) in a 250 mL round bottom flask at 0 °C for 2 h with stirring. The precipitate was recovered by putting the solution on a rotavap and carefully removing the solvents at 50 °C. The product of methylammonium iodide (CH_3NH_3I) or methylammonium bromide (CH_3NH_3Br) was washed with ethanol by stirring the mixture for 30 min. Then, the mixture was filtered and washed three times with diethylether. After filtration, the solid was collected and dried at 70 °C in a vacuum oven for 24 h.

Device fabrication

The substrate of the device was a SNO_2: F (FTO) conducting glass (15 $\Omega\ cm^{-1}$), Pilkington. A blocking layer was deposited on the FTO glass using a solution of titanium diisopropoxidebis(acetylacetonate) (TiDIP, 75% in isopropanol, Aldrich) in ethanol. The TiDIP solution was spin coated and then annealed at 450 °C for 35 min. The TiO_2 solution or the Al_2O_3 solution was spin coated and annealed at 500 °C for 30 min, subsequent to $TiCl_4$ treatment for 30 min at 70 °C and annealing at 500 °C for 30 min.

The synthesis of the $CH_3NH_3PbI_3$ and the $CH_3NH_3PbBr_3$ on the TiO_2 surface was carried out by a two-step deposition technique.

First, PbI_2 or $PbBr_2$ was dissolved in DMF and dropped onto the TiO_2 or the Al_2O_3 film and spin coated, followed by annealing at 70 °C for 30 min. In the second step, the cell was dipped into methylammonium solution. Following the dipping step, the samples were annealed at 70 °C for another 30 min. Finally, the back contact was deposited by evaporating 50 nm of gold under pressure of 5×10^{-6} Torr. The active area was 0.09 cm^2.

Photovoltaic characterization

Photovoltaic measurements were made on a New Port system, composed of an Oriel *I–V* test station using an Oriel Sol3A simulator. The solar simulator is class AAA for spectral performance, uniformity of irradiance, and temporal stability. The solar simulator is equipped with a 450 W xenon lamp. The output power is adjusted to match AM1.5 global sunlight (100 mW cm^{-2}). The spectral match classifications are IEC60904-9 2007, JIC C 8912, and ASTM E927-05. *I–V* curves were obtained by applying an external bias to the cell and measuring the generated photocurrent with a Keithley model 2400 digital source meter. The voltage step and delay time of photocurrent were 10 mV and 40 ms, respectively. Oriel IQE-200 was used to determine the monochromatic incident photon-to-electric current conversion efficiency. Under full computer control, light from a 150 W xenon arc lamp was focused through a monochromator in the 300–1800 nm wavelength range onto the photovoltaic cell under the test. The monochromator was incremented through the visible spectrum to generate the IPCE (λ) as defined by IPCE (λ) = 12 400 ($J_{sc}/\lambda\varphi$), where λ is the wavelength, J_{sc} is the short-circuit photocurrent density (mA cm^{-2}), and φ is the incident radiative flux (mW cm^{-2}). Photovoltaic performance was measured by using a metal mask with an aperture area of 0.09 cm^2.

Surface photovoltage

Surface photovoltage spectroscopy (SPS) and work function were performed using the SKP5050-SPS040 system. The contact potential difference (CPD) between the sample and the vibrating tip was measured by the Kelvin probe technique. Samples were measured in a Faraday cage under air environment. For SPS measurements, the samples were illuminated with a 150 W quartz tungsten halogen lamp. The wavelength resolution was 2 nm. Before the measurement, samples were stabilized with a tip for about one hour. The scan direction was from long to short wavelength. The WF was calculated according to:

$$\mathrm{WF_{sample}} = \mathrm{WF_{tip}} - \mathrm{CPD_{(tip-sample)}}.$$

The WF function of the tip was calibrated above the gold stage.

Intensity modulated photovoltage spectroscopy

The photocarrier recombination times at open circuit were measured by intensity modulated photovoltage spectroscopy (IMVS). The IMVS measurements were performed with the Autolab FRA32M LED driver using a cool white light source, illuminating from the substrate side. The photovoltaic cells were illuminated with a bias light intensity with a 10% sinusoidal wave modulation, with frequencies ranging from 1 Hz to 20 kHz.

High resolution scanning electron microscopy (HR-SEM). The images were obtained using Sirion HR-SEM of FEI (Field Emission Instruments), The Netherlands. The measurement conditions were 5 kV at various magnifications, as seen on the data bar of the images.

Acknowledgements

We would like to thank the Israel Alternative Energy Foundation (I-SAEF) that financed this research, the Ministry of Industry

Trade and Labor Office of the Chief Scientist Kamin project no. 50303, and the Tashtiot project of the Office of the Chief Scientist.

References

1 http://www.nrel.gov/ncpv/images/efficiency_chart.jpg.

2 M. Lee, M. J. Teuscher, T. Miyasaka, T. N. Murakami and H. J. Snaith, Efficient Hybrid Solar Cells Based on Meso-Superstructured Organometal Halide Perovskites, *Science*, 2012, **338**, 643–644.

3 J. M. Ball, M. M. Lee, A. Hey and H. J. Snaith, Low-temperature processed meso-superstructured to thin-film perovskite solar cells, *Energy Environ. Sci.*, 2013, **6**, 1739–1743.

4 J. H. Heo, S. HyukIm, J. H. Noh, T. N. Mandal, C.-S. Lim, J. A. Chang, Y. H. Lee, H.-j. Kim, A. Sarkar, Md. K. Nazeeruddin, M. Grätzel and S. I. Seok, Efficient inorganic–organic hybrid heterojunction solar cells containing perovskite compound and polymeric hole conductors, *Nat. Photonics*, 2013, **7**, 486–491.

5 S. D. Stranks, G. E. Eperon, G. Grancini, C. Menelaou, M. J. P. Alcocer, T. Leijtens, L. M. Herz, A. Petrozza and H. J. Snaith, Electron–Hole Diffusion Lengths Exceeding 1 Micrometer in an Organo metal Trihalide Perovskite Absorber, *Science*, 2013, **342**, 341.

6 G. Xing, N. Mathews, S. Sun, S. S. Lim, Y. M. Lam, M. Grätzel, S. Mhaisalkar and T. C. Sum, Long-Range Balanced Electron- and Hole-Transport Lengths in Organic–Inorganic $CH_3NH_3PbI_3$, *Science*, 2013, **342**, 344.

7 L. Etgar, P. Gao, Z. Xue, Q. Peng, A. K. Chandiran, B. Liu, K. Nazeeruddin and M. Grätzel, Mesoscopic $CH_3NH_3PbI_3$/TiO_2 Heterojunction Solar Cells, *J. Am. Chem. Soc.*, 2012, **134**, 17396–17399.

8 W. A. Laben and L. Etgar, Depleted hole conductor-free lead halide iodide heterojunction solar cell, *Energy Environ. Sci.*, 2013, **6**, 3249–3253.

9 S. Aharon, S. Gamliel, B. El Cohen and L. Etgar, *Phys. Chem. Chem. Phys.*, 2014, **16**, 10512.

10 B. Cai, Y. Xing, Z. Yang, W.-H. Zhang and J. Qiu, High performance hybrid solar cells sensitized by organolead halide perovskites, *Energy Environ. Sci.*, 2013, **6**, 1480.

11 E. Edri, S. Kirmayer, D. Cahen and G. Hodes, High Open-Circuit Voltage Solar Cells Based on Organic–Inorganic Lead Bromide Perovskite, *J. Phys. Chem. Lett.*, 2013, **4**, 897–902.

12 E. Edri, S. Kirmayer, M. Kulbak, G. Hodes and D. Cahen, Chloride Inclusion and Hole Transport Material Doping to Improve Methyl Ammonium Lead Bromide Perovskite-Based High Open-Circuit Voltage Solar Cells, *J. Phys. Chem. Lett.*, 2014, **5**, 429–433.

13 S. Ryu, J. H. Noh, N. J. Jeon, Y. C. Kim, W. S. Yang and J. w. S. S. Il Seok, Voltage output of efficient perovskite solar cells with high open-circuit voltage and fill factor, *Energy Environ. Sci.*, 2014, **7**, 2614–2618.

14 B.-E. Cohen, S. Gamliel and L. Etgar, Parameters influencing the deposition of methylammonium lead halide iodide in hole conductor free perovskite-based solar cells, *APL Mater.*, 2014, **2**, 081502.

15 J. Burschka, N. Pellet, S.-J. Moon, R. Humphry-Baker, P. Gao, M. K. Nazeeruddin and M. Graetzel, *Nature*, 2013, **499**, 316.

16 Y.-F. Chiang, J.-Y. Jeng, M.-H. Lee, S.-R. Peng, P. Chen, T.-F. Guo, T.-C. Wen, Y.-J. Hsu and C.-M. Hsu, High voltage and efficient bilayer heterojunction solar cells based on an organic–inorganic hybrid perovskite absorber with a low-cost flexible substrate, *Phys. Chem. Chem. Phys.*, 2014, **16**, 6033.

17 H.-S. Kim, I. Mora-Sero, V. Gonzalez-Pedro, F. Fabregat-Santiago, E. J. Juarez-Perez, N.-G. Park and J. Bisquert, Mechanism of carrier accumulation in perovskite thin-absorber solar cells, *Nat. Commun.*, 2013, **4**, 2242.

18 K. Zhu, S.-R. Jang and A. J. Frank, Impact of High Charge-Collection Efficiencies and Dark Energy-Loss Processes on Transport, Recombination, and Photovoltaic Properties of Dye-Sensitized Solar Cells, *J. Phys. Chem. Lett.*, 2011, **2**, 1070–1076.

19 Y. Zhao and K. Zhu, Charge Transport and Recombination in Perovskite $(CH_3NH_3)PbI_3$ Sensitized TiO_2 Solar Cells, *J. Phys. Chem. Lett.*, 2013, **4**, 2880–2884.

20 Y. Zhao, A. M. Nardes and K. Zhu, Solid-State Mesostructured Perovskite $CH_3NH_3PbI_3$ Solar Cells: Charge Transport, Recombination, and Diffusion Length, *J. Phys. Chem. Lett.*, 2014, **5**, 490–494.

21 A. J. Mozer, P. Wagner, D. L. Officer, G. G. Wallace, W. M. Campbell, M. Miyashita, K. Sunaharac and S. Mori, The origin of open circuit voltage of porphyrin-sensitised TiO_2 solar cells, *Chem. Commun.*, 2008, 4741–4743.

22 P. Docampo, P. Tiwana, N. Sakai, H. Miura, L. Herz, T. Murakami and H. J. Snaith, Unraveling the Function of an MgO Interlayer in Both Electrolyte and Solid-State SnO_2 Based Dye-Sensitized Solar Cells, *J. Phys. Chem. Lett.*, 2014, **5**, 490–494.

23 J. HyoekIm, J. Chung, S.-J. Kim and N.-G. Park, Synthesis, structure, and photovoltaic property of a nanocrystalline 2H perovskite-type novel sensitizer $(CH_3CH_2NH_3)PbI_3$, *Nanoscale Res. Lett.*, 2012, **7**, 353.

24 S. Aharon, B. E. Cohen and L. Etgar, Hybrid Lead Halide Iodide and Lead Halide Bromide in Efficient Hole Conductor Free Perovskite Solar Cell, *J. Phys. Chem. C*, 2014, **118**(30), 17160–17165.